

Study of Conformally Flat Initial Data for Highly Spinning Black Holes and their Early Evolutions

Carlos O. Lousto, Hiroyuki Nakano, Yosef Zlochower, Bruno C. Mundim, Manuela Campanelli

*Center for Computational Relativity and Gravitation,
and School of Mathematical Sciences, Rochester Institute of Technology,
85 Lomb Memorial Drive, Rochester, New York 14623*

We study conformally-flat initial data for an arbitrary number of spinning black holes with exact analytic solutions to the momentum constraints constructed from a linear combination of the classical Bowen-York and conformal Kerr extrinsic curvatures. The solution leading to the largest intrinsic spin, relative to the ADM mass of the spacetime $\epsilon_S = S/M_{\text{ADM}}^2$, is a superposition with relative weights of $\Lambda = 0.783$ for conformal Kerr and $(1 - \Lambda) = 0.217$ for Bowen-York. In addition, we measure the spin relative to the initial horizon mass M_{H_0} , and find that the quantity $\chi = S/M_{H_0}^2$ reaches a maximum of $\chi^{\text{max}} = 0.9856$ for $\Lambda = 0.753$. After equilibration, the final black-hole spin should lie in the interval $0.9324 < \chi_{\text{final}} < 0.9856$. We perform full numerical evolutions to compute the energy radiated and the final horizon mass and spin. We find that the black hole settles to a final spin of $\chi_{\text{final}}^{\text{max}} = 0.935$ when $\Lambda = 0.783$. We also study the evolution of the apparent horizon structure of this *maximal* black hole in detail.

PACS numbers: 04.25.dg, 04.30.Db, 04.25.Nx, 04.70.Bw

I. INTRODUCTION

With the breakthroughs in the numerical techniques to evolve black-hole binaries (BHBs) [1–3], Numerical Relativity (NR) has become a very important tool to explore highly-dynamical and nonlinear predictions of General Relativity. NR can now be used to evolve generic black-hole binaries and accurately compute gravitational radiation from such systems. However, these computations are very costly when one explores various corners of the BHB parameter space, such as extreme mass ratios and nearly maximally spinning black holes. Yet those cases are of great astrophysical interest [4]. Recently, BHBs with a mass ratio of 1:100 were successfully simulated [5–7], and equal-mass BHBs with spin parameters up to at least 0.97 of the maximum spin were evolved for 25 orbits [8]. These latter simulations used the first order generalized harmonic formalism and excision of the black-hole (BH) interiors in a pseudospectral evolution scheme.

Simulations of highly-spinning black holes are important for understanding astrophysical black holes. Important spin effects have been found in the merger of BHBs, such as the hangup effect [9], large recoil velocities of up to 5000km/s [10], and their statistical consequences for galaxy merger [11]. Recent observational evidence for highly recoiling black holes was reviewed in Ref. [12].

Many of the groups in numerical relativity have adopted the so called, moving punctures formalism [2, 3], where the interiors of the black holes are evolved without imposing internal boundary conditions. Since this approach usually starts from conformally flat puncture [13] initial conditions, and since there is a proof (under the assumption of axisymmetry and that such a slicing should vary smoothly with the spin parameter a) of the nonexistence of conformally flat slices of a Kerr black hole [14], it is generally believed that these data cannot represent

highly-spinning black holes. However, the above statement is not quantitative, nor does it take into account the other “half” of the initial data, i.e. the extrinsic curvature. Even if we could find slices that make the Kerr metric conformally flat, they would presumably not be maximal, i.e. $K \neq 0$. This means that the Hamiltonian and momentum constraints would couple, making the latter nonlinear and superposition of solutions no longer valid.

The first and most widely used initial extrinsic curvature data for spinning black holes is the Bowen-York (BY) solution [15] to the momentum constraints. This assumes a conformally flat 3-metric and a longitudinal, trace-free extrinsic curvature. Cook and York [16] studied intrinsic spins of these data [normalized to the square of Arnowitt-Deser-Misner (ADM) mass [17] (ADM) mass of the spacetime], $\epsilon_S = S/M_{\text{ADM}}^2$, and found that ϵ_S approaches a maximum value of $\epsilon_{S\text{BY}}^{\text{max}} = 0.928$. Further increases of the spin for these data leads to a corresponding increase in the ADM mass such that the intrinsic spin is unchanged. Later, in Ref. [18], it was shown that the conformal extrinsic curvature of a Kerr BH was also an exact solution to the conformally flat momentum constraints. We denote such initial data by “cKerr” to distinguish them from the true Kerr initial data. Those solutions have a maximum intrinsic spin of $\epsilon_{S\text{cKerr}}^{\text{max}} = 0.932$. This raises the possibility that, by choosing a different extrinsic curvature, one can reach still higher maximum values of the intrinsic spin, while keeping the conformal flatness condition for the initial 3-metric. In this paper we will explore this possibility explicitly. Assuming the optimal extrinsic curvature is still close to that of a Kerr BH, we will study a parametrization of deviations from the conformal Kerr extrinsic curvature proportional to the difference between the conformal Kerr and BY extrinsic curvatures. This plays the role of a sourceless extrinsic

curvature *wave*. We also perform high resolution evolutions that allow us to shed some light on the transition from the near maximally spinning conformally flat initial data to the final submaximal spinning Kerr black hole. In particular we track the evolution of trapped surfaces and apparent horizons.

II. INITIAL VALUE PROBLEM FOR BLACK HOLES

We assume a conformally flat 3-metric for the initial configuration

$$\gamma_{ij} = \psi^4 \tilde{\gamma}_{ij}, \quad (1)$$

where $\tilde{\gamma}_{ij}$ is a conformal 3-metric and the 3-Ricci tensor $\tilde{R}_{ij} = 0$. The physical extrinsic curvature is given by $K_{ij} = \psi^{-2} \tilde{K}_{ij}$, and $K^{ij} = \psi^{-10} \tilde{K}^{ij}$. The indices are raised and lowered with the conformal 3-metric $\tilde{\gamma}_{ij}$. $\tilde{\nabla}_i$ is the covariant derivative with respect to the conformal 3-metric $\tilde{\gamma}_{ij}$.

Assuming the maximal slicing $\tilde{K} = \tilde{K}_i^i = 0$, the momentum constraint becomes,

$$\tilde{\nabla}^j \tilde{K}_{ij} = 8\pi \tilde{j}_i, \quad (2)$$

where \tilde{j}_i is a conformal matter momentum density, and the physical matter momentum density is given by $j_i = \psi^{-6} \tilde{j}_i$.

The Hamiltonian constraint leads to

$$\Delta\psi + \frac{1}{8} \tilde{K}_{ij} \tilde{K}^{ij} \psi^{-7} = 0, \quad (3)$$

where, for conformally flat initial data, Δ is the ordinary Laplacian operator. Taking $\psi = 1 + m_p/(2r) + u(\vec{x})$, where m_p is a parameter, $r = |\vec{x}|$, and $u(\vec{x})$ is continuous function (in fact, C^2) leads to unique solutions of the Hamiltonian constraint.

To solve the momentum constraint in Eq. (2), we split the conformal extrinsic curvature \tilde{K}_{ij} into a transverse-traceless and longitudinal part [19] of the form

$$\tilde{K}_{ij} = (\mathbb{L}V)_{ij} + T_{ij}, \quad (4)$$

where the operator \mathbb{L} is given by

$$(\mathbb{L}V)_{ij} = 2\tilde{\nabla}_{(i} V_{j)} - \frac{2}{3} \delta_{ij} \tilde{\nabla}_k V^k, \quad (5)$$

and T_{ij} is a symmetric, transverse-traceless tensor,

$$\tilde{\nabla}^j T_{ij} = 0, \quad T_i^i = 0. \quad (6)$$

Here V_i must be a solution of

$$\tilde{\nabla}^j (\mathbb{L}V)_{ij} = 8\pi \tilde{j}_i. \quad (7)$$

The spinning BY extrinsic curvature [15] is obtained from the vector field

$$V^i = \frac{1}{r^2} \epsilon^{ijk} n_j S_k, \quad (8)$$

where $n^i = x^i/r$ in the Cartesian coordinates $\{x, y, z\}$, S^i is a spin vector, and the Levi-Civita symbol is defined as $\epsilon^{xyz} = \epsilon_{xyz} = 1$. When we include $r = 0$ in this analysis, the momentum constraint becomes

$$\tilde{\nabla}^j \tilde{K}_{ij}^{\text{BY}} = 4\pi \epsilon_{ijk} S^k \tilde{\nabla}^j \delta^{(3)}(x^\ell). \quad (9)$$

If we do not add an additional T_{ij} part, the spinning BY solution is a purely longitudinal solution.

To solve for these initial data numerically, we use the TWO PUNCTURES thorn [20] and the CACTUS/CARPET/EINSTEIN TOOLKIT infrastructure [21–24]. We restrict our analysis here to single BH spacetimes. We solve the Hamiltonian constraint for ψ using the TWO PUNCTURES thorn by setting the mass and spin of the second puncture to zero.

We use AHFINDERDIRECT [25] to locate apparent horizons (AHs). We measure the magnitude of the horizon spin using the Isolated Horizon algorithm detailed in Ref. [26]. Note that once we have the horizon spin, we can calculate the horizon mass via the Christodoulou formula

$$m_H = \sqrt{m_{\text{irr}}^2 + S_H^2/(4m_{\text{irr}}^2)}, \quad (10)$$

where $m_{\text{irr}} = \sqrt{A/(16\pi)}$ and A is the surface area of the horizon, and S_H is the spin angular momentum of the BH (in units of M^2). We denote the horizon mass on the initial slice and the final equilibrated horizon mass by M_{H_0} and M_{H_∞} , respectively.

III. GENERALIZATION OF CONFORMALLY-FLAT INITIAL-DATA

In Ref. [18] it was shown that

$$\tilde{K}_{ij} = \frac{2}{r^2 \sin^4 \theta} [(\hat{S}^a \tilde{\nabla}_a \omega) \epsilon_{k\ell(i} \hat{S}^k n^\ell n_{j)} - (n^a \tilde{\nabla}_a \omega) \epsilon_{k\ell(i} \hat{S}^k n^\ell \hat{S}_{j)}] \quad (11)$$

is a solution to the momentum constraints, where $\cos \theta = \hat{S}^i n_i$ and $\hat{S}^i = S^i/S$, provided that the coordinates are (quasi-) isotropic (i.e. the conformal metric is flat, or conformally Kerr in quasi-isotropic coordinates). The (otherwise arbitrary) scalar function ω gives the angular momentum of the BH [15]. That is, the spin angular momentum J_i is given by

$$\begin{aligned} J_i &= \frac{1}{16\pi} \epsilon_{ijk} \oint_{r=\infty} (x^j K^{km} - x^k K^{jm}) d^2 S_m \\ &= -\frac{\hat{S}_i}{4} \left(\omega(\theta = \pi) - \omega(\theta = 0) \right) \Big|_{r=\infty}, \end{aligned} \quad (12)$$

assuming $\psi \rightarrow 1$ in the limit $r \rightarrow \infty$.

The spinning BY initial data can be recovered by taking

$$\omega_{\text{BY}} = -S (\cos^3 \theta - 3 \cos \theta). \quad (13)$$

On the other hand, Eq. (11) is linear in ω , and we can therefore take an arbitrary superposition $\sum_i c_i \omega_i$, where c_i are constants and each ω_i yields a solution to the vacuum momentum constraint. In particular, we are interested in

$$\delta\omega = \omega^K - \omega^{\text{BY}} = \frac{M_K a^3 \sin^4 \theta \cos \theta}{\Sigma}, \quad (14)$$

where $a = S_{\text{wave}}/M_K$, $\Sigma = (r_{\text{BL}}^2 + a^2 \cos^2 \theta)$ and $r_{\text{BL}} = r[1 + (M_K + a)/(2r)][1 + (M_K - a)/(2r)]$. Here we denote the spin parameter by S_{wave} rather than S because it is in a transverse-traceless “wave-like” part of the extrinsic curvature (see below), and does not contribute to the ADM angular momentum (unlike S). Therefore, it need not match the BH’s spin.

Replacing ω in Eq. (11) by $\delta\omega$ yields a solution to the momentum constraints with zero spin, which we will denote by $\delta\tilde{K}_{ij} = \tilde{K}_{ij}^K - \tilde{K}_{ij}^{\text{BY}}$. We note that $\delta\tilde{K}_{ij}$ is transverse-traceless, i.e., $\tilde{\nabla}^j \delta\tilde{K}_{ij} = 0$ everywhere, because it is constructed from the difference of two extrinsic curvatures each leading to the same source term \tilde{j}_i in Eq. (2). Finally, the extrinsic curvature given by $\tilde{K}_{ij} = \tilde{K}_{ij}^{\text{BY}} + \Lambda \delta\tilde{K}_{ij}$ solves the momentum constraints, with non-zero spin, for any fixed value of Λ . Taking $\Lambda = 1$ yields a pure conformal Kerr extrinsic curvature (provided that one uses the same spin parameter $S_{\text{wave}} = S$ to construct $\tilde{K}_{ij}^{\text{BY}}$ and $\delta\tilde{K}_{ij}$), while $\Lambda = 0$ corresponds to pure BY curvature. Again, we note that $\delta\tilde{K}_{ij}$ does not contribute to the spin, so in principle, one can use a different spin parameter to construct $\tilde{K}_{ij}^{\text{BY}}$ and $\delta\tilde{K}_{ij}$.

IV. ANALYSIS OF SINGLE SPINNING BLACK HOLE INITIAL DATA

The extrinsic curvature in Eq. (11) can be written as

$$\tilde{K}_{ij} = \frac{2}{r} [(\alpha_\theta - (\hat{S}^m n_m)^2 \alpha_r) \epsilon_{k\ell(i} \hat{S}^k n^\ell n_{j)} + \alpha_r (\hat{S}^m n_m) \epsilon_{k\ell(i} \hat{S}^k n^\ell \hat{S}_{j)}], \quad (15)$$

where the coefficients α_θ and α_r are given by

$$\alpha_\theta^{\text{BY}} = \frac{3S}{r^2}, \quad \alpha_r^{\text{BY}} = 0, \quad (16)$$

for the BY case, and for $\delta\omega$ we have

$$\begin{aligned} \delta\alpha_\theta &= -16 M_K a^3 [(-40 r M_K a^2 + 5 a^4 + 5 M_K^4 \\ &\quad - 10 M_K^2 a^2 + 80 r^4 - 24 r^2 a^2 + 40 r M_K^3 \\ &\quad + 160 r^3 M_K + 120 r^2 M_K^2) \cos^2 \theta \\ &\quad - (2r + M_K + a)^2 (2r + M_K - a)^2 \\ &\quad + 48 a^2 r^2 \cos^4 \theta] / \beta^2, \\ \delta\alpha_r &= 32 M_K a^3 (2r + M_K + a) (2r + M_K - a) \\ &\quad \times (a^2 - M_K^2 + 4r^2) / \beta^2, \end{aligned} \quad (17)$$

where

$$\begin{aligned} \beta &= 16 r^2 \Sigma \\ &= 16 r^4 + M_K^4 + a^4 + 24 r^2 M_K^2 - 8 r^2 a^2 \\ &\quad + 8 r M_K^3 - 2 M_K^2 a^2 - 8 r M_K a^2 \\ &\quad + 32 r^3 M_K + 16 a^2 r^2 \cos^2 \theta. \end{aligned} \quad (18)$$

As a way to study the effects of changing the extrinsic curvature on the maximum intrinsic spins, we set the conformal extrinsic curvature to

$$\tilde{K}_{ij} = \tilde{K}_{ij}^{\text{BY}} + \Lambda \delta\tilde{K}_{ij}, \quad (19)$$

and vary the parameters Λ , M_K , and the spin parameter $S_{\text{wave}} = M_K a$ used to construct $\delta\tilde{K}_{ij} = (\tilde{K}_{ij}^K - \tilde{K}_{ij}^{\text{BY}})$. In all cases the spin used to construct $\tilde{K}_{ij}^{\text{BY}}$ remains fixed at $S = M^2$.

A. ADM mass dependence

To estimate the final (equilibrated) the intrinsic spin for a large number of configurations, we measure the ADM mass of a single spinning BH spacetime with spin parameter $S = M^2$ and puncture mass $m_p = 0.02M$. We choose this puncture mass so that it has a negligible effect on the total ADM mass, while still leading to a solvable initial data problem (taking $m_p = 0$ would lead to singularities at the puncture). For the sequences presented here, we only perform numerical evolutions to calculate the equilibrated spin on a select set of configurations. For the rest, we note that equilibrated value of the intrinsic spin $S_H/M_{H_\infty}^2$ (as measured using the equilibrated horizon mass) must be larger than S_H/M_{ADM}^2 , which holds true because these axisymmetric data can radiate mass but not angular momentum. Since the total mass radiated is small ($\delta M/M < 0.2\%$) [18], S_H/M_{ADM}^2 is a reasonable approximation for the final spin. One might expect that the conformal Kerr extrinsic curvature leads to the largest intrinsic spin, but as shown in Fig. 1, the actual minimum in the ADM mass occurs at $\Lambda = 0.7831$, or roughly a mixture of 78% conformal Kerr and 22% BY extrinsic curvatures. As seen in Fig. 2, if we take $\Lambda = 0.7831$ and vary the mass parameter M_K in the extrinsic curvature (note that this is not the mass of the BH, rather it is the proportionality factor between S_{wave} and the Kerr a parameter in the extrinsic curvature $\delta\tilde{K}_{ij}$) we find that the ADM mass is minimized when $M_K = M$. On the other hand, if we take $\Lambda = 1$, the ADM mass is minimized at slightly larger values of M_K . Finally, we need not have the spin of the wave (i.e. the spin parameter in $\delta\tilde{K}_{ij}$) match the BY spin. In Fig. 3 we plot the ADM mass for a BH of spin $S = M^2$ and vary the “spin” of the curvature wave. The minimum in the ADM mass occurs when $S_{\text{wave}} = S$ when $\Lambda = 0.7831$ and at slightly smaller values for $\Lambda = 1$ (note that $\Lambda = 1$ only correspond to pure conformal Kerr data when $S_{\text{wave}} = S$).

The smallest ADM mass, and therefore the largest intrinsic spins, are obtained when $S_{\text{wave}} = S$, $M_K = M$, and $\Lambda = 0.7831$. The corresponding spin is $S_H/M_{\text{ADM}}^2 = 0.9324$, which is slightly larger than the maximum spin of 0.932 obtained from purely conformal Kerr extrinsic curvature.

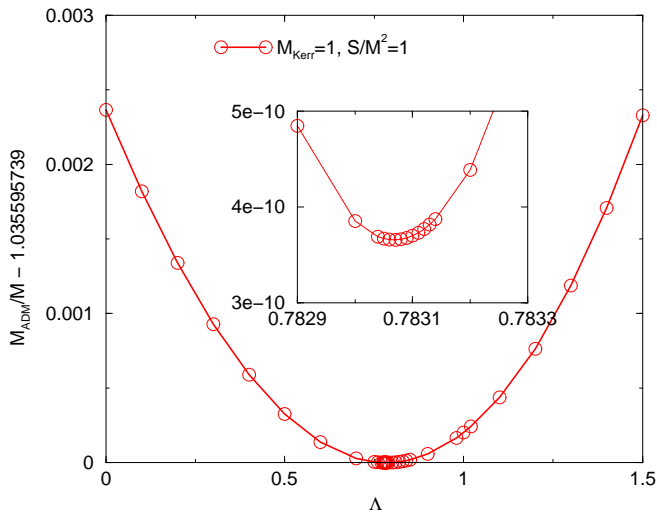


FIG. 1: The ADM mass of a single spinning BH with spin parameter $S = M^2$ versus weight Λ . Here the spin of the wave $\delta\tilde{K}_{ij}$ is fixed at $S_{\text{wave}} = M^2$. Note that $\Lambda = 1$, which corresponds to conformal Kerr extrinsic curvature, does not lead to the minimum mass, and hence maximum intrinsic spin.

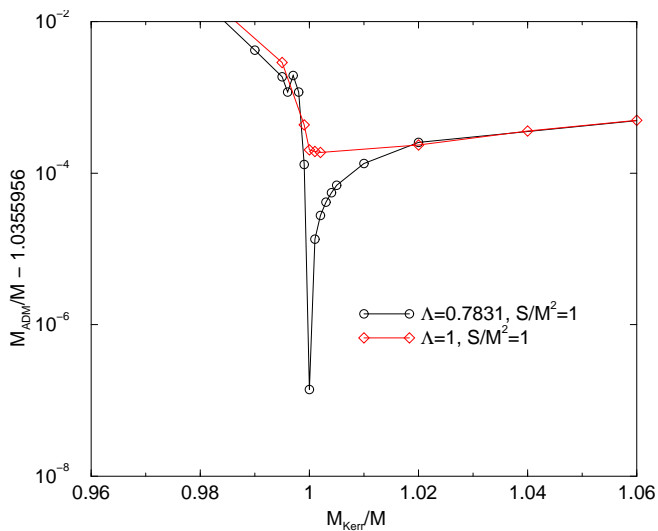


FIG. 2: The ADM mass of a single spinning BH with spin parameter $S = M^2$ as a function of the Kerr mass parameter in the extrinsic curvature wave. Here the spin of the wave $\delta\tilde{K}_{ij}$ is fixed at $S_{\text{wave}} = M^2$. A minimum in the ADM mass is obtained for $M_K = 1$ when $\Lambda = 0.7831$. The minimum is at slightly larger values of M_K for pure conformal Kerr extrinsic curvature.

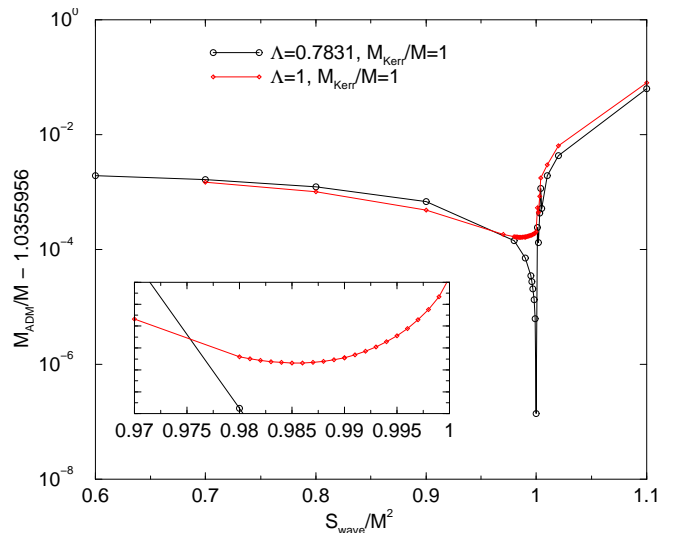


FIG. 3: The ADM mass of a spinning BH with spin parameter $S = M^2$ as a function of spin of the curvature wave S_{wave} for $\Lambda = 0.7831$ and $\Lambda = 1$. Here $M_K = M$.

TABLE I: Initial spin parameters for Bowen-York data (BY), the new data at Λ^{max} , and conformal Kerr data. Note that $\xi = \chi/(1 + \sqrt{1 - \chi^2})$. In all cases, the spin S/M^2 is identically 1.

ID	$\epsilon_S = S/M_{\text{ADM}}^2$	$\chi = S/M_{H_0}^2$	$\xi = S/(2M_{\text{irr}}^2)$
BY	0.9282	0.9831	0.8311
Λ^{max}	0.9324	0.9856	0.8431
cKerr	0.93207	0.9854	0.8421

B. Horizon mass dependence

The difference between the ADM mass and the initial horizon mass of the black holes provides a measure of the energy initially lying outside the horizon. This energy can potentially escape to infinity or be absorbed by the black hole. We thus expect that the evolution of these spinning black holes will lead to a stationary black hole with

$$\epsilon_S^{\text{initial}} = \frac{S}{M_{\text{ADM}}^2} < \chi_{\text{final}} < \chi_{\text{initial}} = \frac{S}{M_{H_0}^2}. \quad (20)$$

For the $\Lambda^{\text{max}} = 0.7831$ case, $0.9324 < \chi_{\text{final}} < 0.9856$. We also investigate the minimum of the horizon mass when Λ is varied but S and M_k are set M^2 and M , respectively. The results are shown in Fig. 4. The minimum horizon mass occurs when $\Lambda^{\text{max}} = 0.753$, which is close to where the minimum in the ADM mass occurs. We summarize the initial parameters in Table I.

V. EVOLUTIONS

We evolve these single (distorted) BH data-sets using the LAZEV [27] implementation of the moving punc-

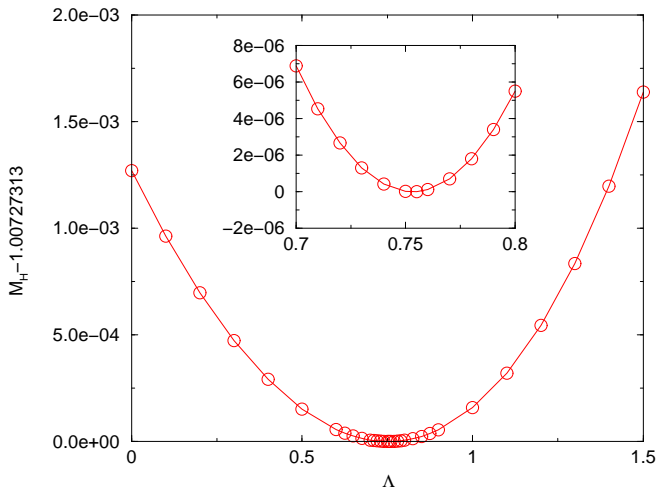


FIG. 4: The horizon mass of a spinning BH with spin parameter $S = M^2$ as a function of Λ , the mixing parameter for BY and conformal Kerr curvatures.

ture approach [2, 3] with the conformal function $W = \exp(-2\phi)$ suggested by Ref. [28]. For the runs presented here, we use centered, eighth-order finite differencing in space [29] and a fourth-order Runge Kutta time integrator. (Note that we do not upwind the advection terms.)

Our code uses the CACTUS/EINSTEINTOOLKIT [21, 22] infrastructure. For these runs, we used the CARPET [24] mesh refinement driver to provide fixed mesh refinement (since the BHs do not move across the grid); initially starting with 15 levels of refinement. When a larger AH forms, we reduce the numbers of levels from 15 to 11. Our base (coarsest) grid extended from $-400M$ to $400M$ in all directions with a resolution of $h = 10M/3$. We used the π and z -reflection symmetries to reduce the computational domain by a factor of 4. The resolution on the finest grid was $h = M/1000$. We took a constant Courant factor of $dt/h = 1/4$ in all grids. We were able to achieve good spin preservation by choosing a grid structure where the finest grid is roughly twice as wide as the AH. Here we extended to finest grid to $\pm 0.021M$.

We found that using a lower-order dissipation operator, in this case fifth-order, gave sufficient accuracy, while, at the same time, reducing the number of required buffer points at the refinement boundary, as well as the cost in walltime of the dissipation step. At these boundaries, we used 16 buffer points. Standard ninth-order dissipation would require 20 buffer zones, while seventh-order would not require additional buffer zones, it proved to give a more noisy waveform than using the fifth-order dissipation stencil.

The initial data are axisymmetric, which we exploit in order to reduce the number of spectral collocation points to $140 \times 140 \times 4$. We then use the full spectral expansion, rather than the much faster interpolation techniques, to transfer the initial data to the numerical grid.

We obtain accurate, convergent waveforms and horizon

TABLE II: Final spin parameters for Bowen-York data (BY), the new data at Λ^{\max} , and conformal Kerr data. Note that $\alpha_H = S_H/M_{H\infty}^2$, $\alpha_{\text{rad}} = J_{\text{ADM}}/(M_{\text{ADM}} - \delta M_{\text{rad}})^2$. The notation of the form $1.23(4 \pm 5)$ used below is shorthand for 1.234 ± 0.005 .

ID	α_H	α_{rad}	$10^3 \delta M_{\text{rad}}$
BY	0.9309(0 \pm 2)	0.9308(4 \pm 1)	1.47(6 \pm 5)
Λ^{\max}	0.935(2 \pm 1)	0.9351(3 \pm 1)	1.49(1 \pm 6)
cKerr	0.9348(2 \pm 1)	0.9347(6 \pm 2)	1.49(0 \pm 7)
ID	$M_{H\infty}$	S_H	M_{irr}
BY	1.0365(1 \pm 3)	1.0001(5 \pm 5)	0.8563(6 \pm 3)
Λ^{\max}	1.0341(5 \pm 7)	1.000(2 \pm 1)	0.850(9 \pm 1)
cKerr	1.0343(1 \pm 2)	1.0000(8 \pm 4)	0.85138(9 \pm 5)

parameters by evolving this system in conjunction with a modified 1+log lapse and a modified Gamma-driver shift condition [2, 30, 31], and an initial lapse $\alpha(t=0) = 2/(1 + \psi_{BL}^4)$. The lapse and shift are evolved with

$$(\partial_t - \beta^i \partial_i)\alpha = -2\alpha K, \quad (21a)$$

$$\partial_t \beta^a = (3/4)\bar{\Gamma}^a - \eta \beta^a, \quad (21b)$$

where we use $\eta = 1$ for all simulations presented below.

The initial AH spherical and very small (see Fig. 5), with coordinate radius $r \sim 0.009$. A larger AH forms after the BH absorbs the excess radiation on the grid, leading to an oblate spheroid AH with coordinate radius $\sim 0.3 - 0.5$. We drop levels of refinement once this larger AH begins to equilibrate.

We measure radiated energy in terms of the radiative Weyl scalar ψ_4 , using the formulas provided in Refs. [32, 33]. However, rather than using the full ψ_4 , we decompose it into ℓ and m modes and solve for the radiated linear momentum, dropping terms with $\ell \geq 5$. The formulas in Refs. [32, 33] are valid at $r = \infty$. We extract the radiated energy-momentum at finite ($r = 50M, 60M, \dots, 100M$) radius and extrapolate to $r = \infty$ using both linear and quadratic extrapolations. We use the difference of these two extrapolations as a measure of the error.

The initial 3-metric for these black holes is equivalent to the Kerr 3-metric (in quasi-isotropic coordinate) with a non-trivial axisymmetric distortion wave. This initial distortion contains energy that is partially radiated to infinity and partially absorbed by the black hole. From Table I we see that in the extreme case 2.8% of the total mass lies outside the black hole (here $S = 1$)

$$\begin{aligned} M_{\text{ADM}} - M_{H_0} &= \sqrt{\frac{S}{\epsilon_S}} - \sqrt{\frac{S}{\chi}} \\ &= 1.0356 - 1.0073 \\ &= 0.0283. \end{aligned} \quad (22)$$

This difference, $E_{\text{wave}} = M_{\text{ADM}} - M_{H_0}$, is the energy associated with the distortion wave. From Table II, we see that 95% of the energy in the wave is eventually absorbed by the black hole. Of the total ADM mass, only

0.15% is actually radiated to infinity. This means that the black hole transitions from a nearly maximally spinning object to a submaximal Kerr black hole with spin 0.935, as shown in the above Table II. This effect is also shown in Fig. 5, where, at around $t = 10.7M$ of the evolution, a new external AH appears suddenly with a larger area and much larger coordinate radius. Initially, only one trapped surface exists, with a very small coordinate radius of $0.0095M$. As the evolution proceeds this horizon acquires an oblate form with the equatorial radius nearly double the polar radius. The jagged features associated with the smaller trapped surface at later times are due to poor resolution of this very small object (which reduces in polar radius from $\sim 0.009M$ to $< 0.002M$). At $t = 10.7M$ an outer AH forms with polar radius $\sim 0.14M$ and equatorial radius $0.27M$. At the same time a third, shrinking trapped surface also appears that eventually meets the original smaller trapped surface, after $t = 28.2M$. These newly formed horizons are oblate. We can also observe notable quasinormal oscillations soon after their formation.

In order to understand the jump in the area in Fig. 5 when the initial distortion is absorbed by the rotating hole we note that

$$\begin{aligned} \frac{A_H}{S} &= \frac{8\pi}{\xi} \\ &= 8\pi \frac{1 + \sqrt{1 - \chi^2}}{\chi}, \end{aligned} \quad (23)$$

where A_H is the area of the horizon. By keeping S fixed and allowing M_H to vary, we obtain

$$\frac{\delta A_H}{A_H} = \frac{2}{\sqrt{1 - \chi^2}} \left(\frac{\delta M_H}{M_H} \right). \quad (24)$$

In our case this leads to a relative increase in the horizon area of 15% = $5.64 \times 2.685\%$ (using the numbers of Table II) in agreement with the 12.4 – 18.1% jump observed in the bottom plot of Fig. 5 (from 29.8 initially to 34 and then to 36.4) for the A_H . Another interesting aspect of these horizons is the jump in the deviation from nearly spherical to spheroidal. We define the deviation functions D to measure the non-spherical shape of the horizons. We define the coordinate dependent deviation $D_r = (r_{\text{equatorial}} - r_{\text{polar}})/(r_{\text{equatorial}} + r_{\text{polar}})$, where r is the coordinate radius, and coordinate independent deviation $D_c = (c_{\text{equatorial}} - c_{\text{polar}})/(c_{\text{equatorial}} + c_{\text{polar}})$, where c is the invariant measure of the circumference (see [34] for formulas relating D_c to the intrinsic spin a/M for Kerr). For a spherical horizon, D_c must be zero in all coordinate systems, while D_r can differ from zero, with the difference being a measure of how distorted the coordinate system is in the neighborhood of the AH.

The initial horizon is highly spinning. Therefore, we would expect it to show the largest deviation from spherical. However, as seen in Fig. 6, this horizon is more spherical (i.e. $|D_c|$ is smaller) than the slower spinning equilibrium horizon (slower in the sense S/M_H^2 is smaller,

S itself is constant). Also note that the distortion of the coordinates, as measured by the relative difference between the D_c and D_r are much smaller for the equilibrium horizon despite the fact that this horizon is less spherical. We also observe a notable constancy of D_c of the smallest horizon, beginning from the initial time slice, through the formation of the outer apparent horizon, even until later times when the shrinking internal horizon meets the inner horizon at around $t = 28.2M$. As expected the outer horizon is very distorted when it first forms and then settles to the D_c of a Kerr horizon with the corresponding spinning parameter $a/M = 0.935$.

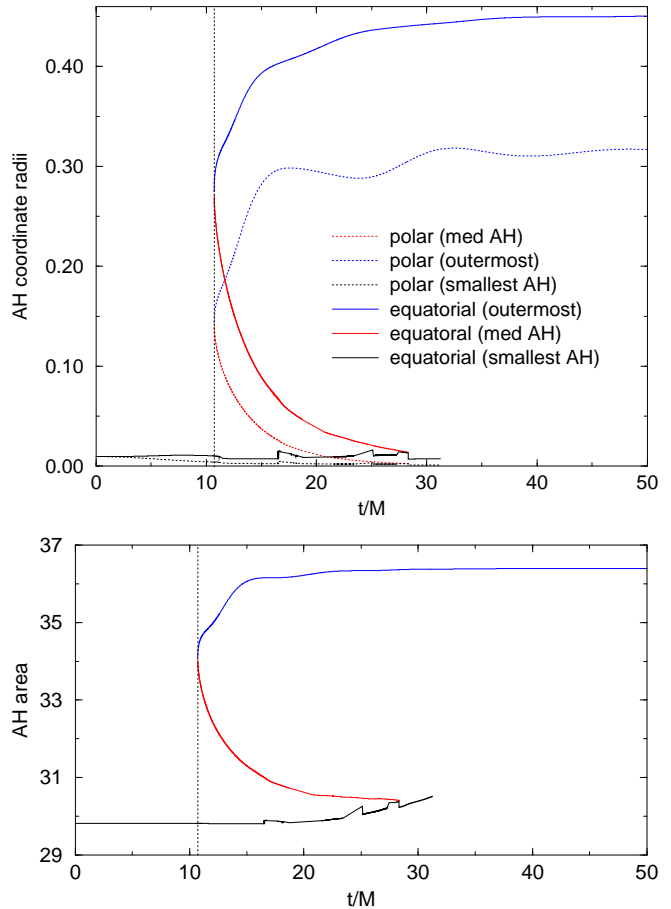


FIG. 5: (Top) The polar and equatorial radii of the three AHs found for the $\Lambda = 0.7831$ data. (Bottom) The area of the same three AHs. All in units of the ADM mass. The dotted vertical line at $t = 10.7M$ represents the time when an external trapped surface first forms.

In Figs. 7 and 8 and Table III, we show the waveform and radiated energy per ℓ mode for pure BY, Λ^{max} and cKerr extrinsic curvature data. Note how for all modes with $\ell > 2$, the cKerr data radiated the most, while pure BY data radiates the least. The effect, however, is essentially in the higher ℓ modes. For the Λ^{max} data, the ADM mass is lower than for BY, and the system radiates more than BY. Both effects lead to larger final spins for the Λ^{max} data when compared to BY data.

TABLE III: The energy radiated ($\delta E/M$), per ℓ mode, for the BY, Λ^{\max} , and cKerr data. Note that the BY data radiates the most in the $\ell = 2$ mode, but least in all other modes. The total radiated energy ($\delta E/M$) over all modes is $(1.4799 \pm 0.0010) \times 10^{-3}$, $(1.4978 \pm 0.0010) \times 10^{-3}$, $(1.4983 \pm 0.0010) \times 10^{-3}$ for BY, Λ^{\max} , and cKerr, respectively.

Mode	BY	Λ^{\max}	cKerr
(2,0)	$(1.416 \pm 0.001) \times 10^{-3}$	$(1.349 \pm 0.001) \times 10^{-3}$	$(1.318 \pm 0.001) \times 10^{-3}$
(3,0)	$(6.01 \pm 0.01) \times 10^{-5}$	$(1.392 \pm 0.005) \times 10^{-4}$	$(1.672 \pm 0.007) \times 10^{-4}$
(4,0)	$(3.56 \pm 0.11) \times 10^{-6}$	$(8.85 \pm 2.8) \times 10^{-6}$	$(1.200 \pm 0.039) \times 10^{-5}$
(5,0)	$(3.12 \pm 0.30) \times 10^{-7}$	$(5.38 \pm 0.60) \times 10^{-7}$	$(7.25 \pm 0.86) \times 10^{-7}$
(6,0)	$(1.13 \pm 0.89) \times 10^{-8}$	$(2.63 \pm 1.22) \times 10^{-8}$	$(3.88 \pm 2.03) \times 10^{-8}$
(7,0)	$(0.3 \pm 1.0) \times 10^{-9}$	$(1.19 \pm 1.82) \times 10^{-9}$	$(1.39 \pm 3.58) \times 10^{-9}$

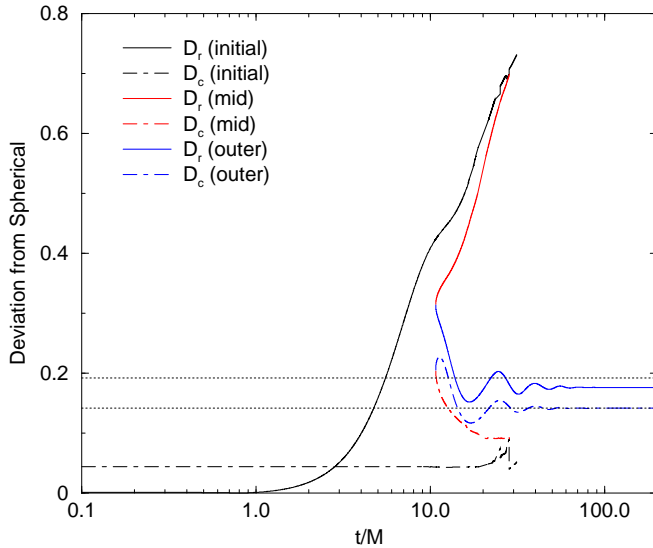


FIG. 6: The deviation of the AH shape from a pure sphere D , for the $\Lambda = 0.7831$ data, as measured using the coordinate radii $D_r = (r_{\text{equatorial}} - r_{\text{polar}})/(r_{\text{equatorial}} + r_{\text{polar}})$ and the coordinate independent measure using the equatorial and polar circumferences $D_c = (c_{\text{equatorial}} - c_{\text{polar}})/(c_{\text{equatorial}} + c_{\text{polar}})$. Note how the initial horizon starts out as a coordinate sphere, which rapidly becomes oblate. While the invariant circumferences indicate a nearly constant deviation from spherical even at $t=0$. The dotted lines show the Kerr values for D_c for the initial intrinsic spin of $\chi_0 = 0.9856$ (upper) and the equilibrium spin of $\chi_\infty = 0.9352$ (lower).

VI. DISCUSSION

In this paper we studied conformally flat initial data with an extrinsic curvature ansatz that interpolates between the Bowen-York solution and the conformal Kerr solution. We found that, given our ansatz, the maximum intrinsic spin, normalized by the ADM mass, does not correspond to a pure conformal Kerr extrinsic curvature, but rather to a weighted sum of roughly 78% conformal Kerr and 22% Bowen-York extrinsic curvatures. While if we normalize the intrinsic spin with the horizon mass,

The Λ^{\max} data, however, does not radiate more than the cKerr data. Thus there is a trade-off between the lower ADM mass of the Λ^{\max} data and total mass radiated for the cKerr data. Slightly smaller final spin could be obtained by optimizing the Λ parameter, but the effect will be quite small. Interestingly, the BY data radiates more in the $\ell = 2$ mode than the other data. It is only after summing over all modes, that the other data sets end up radiated more.

the maximum occurs at roughly 75% conformal Kerr and 25% Bowen-York extrinsic curvatures. This result can be interpreted as implying that, even if the conformal Kerr extrinsic curvature is the ideal choice for conformally Kerr initial data (3-metric), for conformally flat initial data, a mixture including Bowen-York compensates in part for the distortions produced by conformal flatness, leading to slightly larger intrinsic spins.

Other numerical explorations are possible using Eq. (11) above for different choices of ω . One could also try a variational approach, where an extremum in the

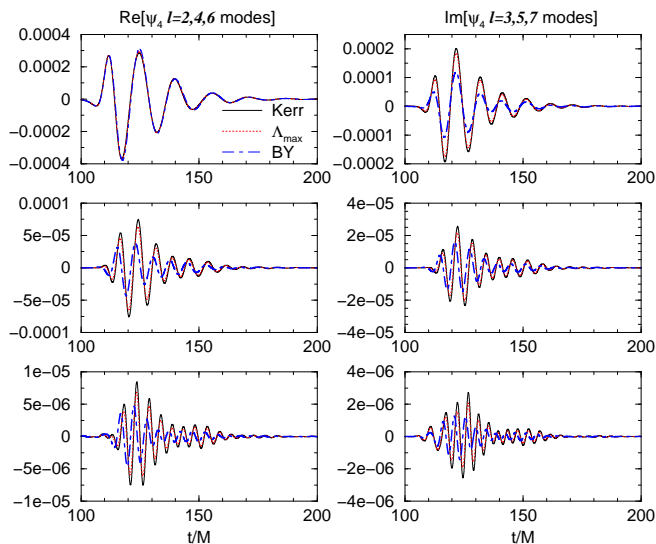


FIG. 7: The $(\ell, 0)$ modes of ψ_4 for the BY, Λ^{\max} , and cKerr data. The plot is arranged in two columns with even ℓ modes to the left and odd ℓ modes to the right. The plots are arranged vertically with lower ℓ modes above higher ℓ modes. For the even ℓ modes, the odd part of ψ_4 is zero and not shown, while for odd ℓ modes, the even part of ψ_4 is zero and not shown. Note how the different initial data give essentially the same $\ell = 2$ signal, but differ quantitatively in the higher ℓ modes.

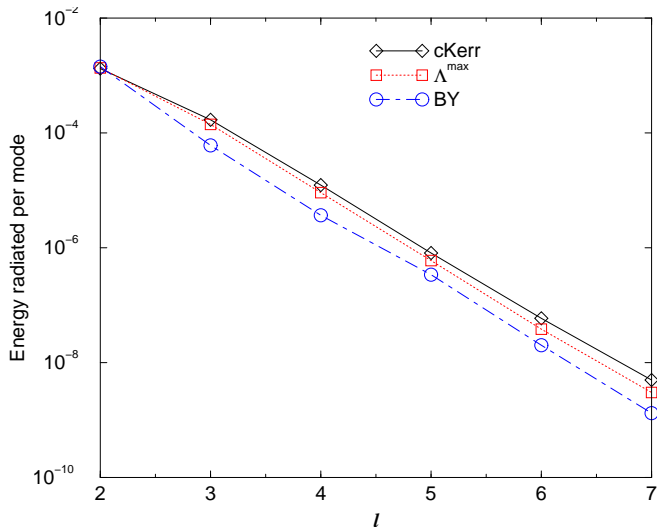


FIG. 8: The energy per $(\ell, 0)$ mode for the BY, Λ^{\max} , and cKerr data.

ADM mass can be found by varying the function ω , but this is beyond the scope of the current paper. Note that Dain and Friedrich [35] have described the general form of the extrinsic curvature for asymptotically flat initial data.

Another example of conformally flat initial data with different extrinsic curvature is provided by the thin-sandwich approach [36], but this requires solving a sys-

tem of five coupled partial differential equations. Our approach is rather to try to keep all the benefits of the simplicity of the Bowen-York solutions, i.e., an analytic conformal extrinsic curvature, Eqs. (15)-(19), with a very simple form that is easy to incorporate in any numerical code that solves the Hamiltonian constraint for the conformal factor. It is the intentions of the authors to deliver an open source code incorporating these new data to the Einstein Toolkit collaboration [23].

Ultimately we are interested in the evolution of these initial data and the ratio $\chi = S/M_H^2$ at late times, since this represents the actual spin of the black holes in a black-hole-binary simulation (that is, the individual black holes will equilibrate on much smaller timescales than the binary inspiral). Our numerical evolutions find that only a small fraction of the available energy initially outside the black hole radiates to infinity. Thus from the two initial data indicators, ϵ_S and χ the former, which is normalized by the ADM mass is the most accurate. We thus conclude that our family of initial data is limited to represent black holes with intrinsic spins $\alpha^{\max} < 0.9352$.

We also find an important jump in the apparent horizon location in numerical coordinates when radiation falls in and the hole settles from an extreme near-spherical horizon to a submaximal Kerr hole with a much larger coordinate size (an increase in coordinate radius of over a factor of 30). One needs to take into account these jumps both in coordinate size and physical mass when designing simulations and especially when measuring properties such as the mass, spin, linear momentum [37], and when tracking the motion of binary horizons in a full numerical simulation. More invariant measures of the horizon properties like its area, Fig. 5, and ratio of polar to equatorial circumferences, Fig. 6, still display an initial quasi-spherical (small distortion) AH, with a discontinuous jump at $t = 10.7M$ to a larger, highly-distorted horizon that, after some oscillation, settles to the spherical deviations corresponding to that of a Kerr hole with $a/M = 0.935$. The moving puncture approach also allows us to keep track of the internal horizon connecting the initial and final ones even after the formation of the latter at $t = 10.7M$. Although the details of this horizon transition are specific of the problem we studied, any other initial data set for multi black holes is expected to have a radiation content that is partially absorbed and partially radiated to infinity, and hence present similar qualitative early evolutions to those presented here.

VII. ACKNOWLEDGMENTS

We thank S. Dain and O. Ortiz for valuable discussions on the subject of this paper. We gratefully acknowledge the NSF for financial support from Grants No. PHY-0722315, No. PHY-0653303, No. PHY-0714388, No. PHY-0722703, No. DMS-0820923, No. PHY-0929114, PHY-0969855, PHY-0903782, and No. CDI-1028087; and NASA for financial support from NASA Grant No.

07-ATFP07-0158. Computational resources were provided by the Ranger cluster at TACC (Teragrid alloca-

tion TG-PHY060027N) and by NewHorizons at RIT.

-
- [1] F. Pretorius, Phys. Rev. Lett. **95**, 121101 (2005), gr-qc/0507014.
- [2] M. Campanelli, C. O. Lousto, P. Marronetti, and Y. Zlochower, Phys. Rev. Lett. **96**, 111101 (2006), gr-qc/0511048.
- [3] J. G. Baker, J. Centrella, D.-I. Choi, M. Koppitz, and J. van Meter, Phys. Rev. Lett. **96**, 111102 (2006), gr-qc/0511103.
- [4] L. Gou, J. E. McClintock, M. J. Reid, J. A. Orosz, J. F. Steiner, et al., Astrophys. J. **742**, 85 (2011), 1106.3690.
- [5] C. O. Lousto and Y. Zlochower, Phys. Rev. Lett. **106**, 041101 (2011), 1009.0292.
- [6] H. Nakano, Y. Zlochower, C. O. Lousto, and M. Campanelli, Phys. Rev. **D84**, 124006 (2011), 1108.4421.
- [7] U. Sperhake, V. Cardoso, C. D. Ott, E. Schnetter, and H. Witek, Phys. Rev. **D84**, 084038 (2011), 1105.5391.
- [8] G. Lovelace, M. Boyle, M. A. Scheel, and B. Szilagyi, Class. Quant. Grav. **29**, 045003 (2012), 1110.2229.
- [9] M. Campanelli, C. O. Lousto, and Y. Zlochower, Phys. Rev. **D74**, 041501(R) (2006), gr-qc/0604012.
- [10] C. O. Lousto and Y. Zlochower, Phys. Rev. Lett. **107**, 231102 (2011), 1108.2009.
- [11] C. O. Lousto, Y. Zlochower, M. Dotti, and M. Volonteri (2012), 1201.1923.
- [12] S. Komossa, Adv. Astron. **2012**, 364973 (2012), 1202.1977.
- [13] S. Brandt and B. Brügmann, Phys. Rev. Lett. **78**, 3606 (1997), gr-qc/9703066.
- [14] A. Garat and R. H. Price, Phys. Rev. **D61**, 124011 (2000), gr-qc/0002013.
- [15] J. M. Bowen and J. W. York, Jr., Phys. Rev. **D21**, 2047 (1980).
- [16] G. B. Cook and J. York, James W., Phys. Rev. **D41**, 1077 (1990).
- [17] R. Arnowitt, S. Deser, and C. W. Misner, in *Gravitation: An Introduction to Current Research*, edited by L. Witten (John Wiley, New York, 1962), pp. 227–265, gr-qc/0405109.
- [18] S. Dain, C. O. Lousto, and R. Takahashi, Phys. Rev. **D65**, 104038 (2002), gr-qc/0201062.
- [19] G. B. Cook, Living Rev. Rel. **3**, 5 (2000), gr-qc/0007085.
- [20] M. Ansorg, B. Brügmann, and W. Tichy, Phys. Rev. **D70**, 064011 (2004), gr-qc/0404056.
- [21] Cactus Computational Toolkit home page: <http://cactuscode.org>.
- [22] Einstein Toolkit home page: <http://einsteintoolkit.org>.
- [23] F. Löffler, J. Faber, E. Bentivegna, T. Bode, P. Diener, et al. (2011), 1111.3344.
- [24] E. Schnetter, S. H. Hawley, and I. Hawke, Class. Quantum Grav. **21**, 1465 (2004), gr-qc/0310042.
- [25] J. Thornburg, Class. Quant. Grav. **21**, 743 (2004), gr-qc/0306056.
- [26] O. Dreyer, B. Krishnan, D. Shoemaker, and E. Schnetter, Phys. Rev. **D67**, 024018 (2003), gr-qc/0206008.
- [27] Y. Zlochower, J. G. Baker, M. Campanelli, and C. O. Lousto, Phys. Rev. **D72**, 024021 (2005), gr-qc/0505055.
- [28] P. Marronetti, W. Tichy, B. Brügmann, J. Gonzalez, and U. Sperhake, Phys. Rev. **D77**, 064010 (2008), 0709.2160.
- [29] C. O. Lousto and Y. Zlochower, Phys. Rev. **D77**, 024034 (2008), 0711.1165.
- [30] M. Alcubierre, B. Brügmann, P. Diener, M. Koppitz, D. Pollney, E. Seidel, and R. Takahashi, Phys. Rev. **D67**, 084023 (2003), gr-qc/0206072.
- [31] J. R. van Meter, J. G. Baker, M. Koppitz, and D.-I. Choi, Phys. Rev. **D73**, 124011 (2006), gr-qc/0605030.
- [32] M. Campanelli and C. O. Lousto, Phys. Rev. **D59**, 124022 (1999), gr-qc/9811019.
- [33] C. O. Lousto and Y. Zlochower, Phys. Rev. **D76**, 041502(R) (2007), gr-qc/0703061.
- [34] M. Alcubierre et al., Phys. Rev. **D72**, 044004 (2005), gr-qc/0411149.
- [35] S. Dain and H. Friedrich, Commun. Math. Phys. **222**, 569 (2001), gr-qc/0102047.
- [36] H. P. Pfeiffer and J. York, James W., Phys. Rev. Lett. **95**, 091101 (2005), gr-qc/0504142.
- [37] B. Krishnan, C. O. Lousto, and Y. Zlochower, Phys. Rev. **D76**, 081501 (2007), 0707.0876.